Title

Hydrothermal synthesis and characterization under dynamic conditions of cobalt oxide nanoparticles supported over magnesium oxide nano-plates

Journal

Dalton Transactions, 45(24)

ISSN

1477-9226

Authors

Alayoglu, Selim

Rosenberg, Daniel J

Ahmed, Musahid

Publication Date

2016-06-14

DOI

10.1039/c6dt00204h

Peer reviewed

Hydrothermal Synthesis and Characterization under Dynamic Conditions of Cobalt Oxide Nanoparticles Supported over Magnesium Oxide Nano-plates

*Selim Alayoglu, Daniel J. Rosenberg and Musahid Ahmed

Chemical Sciences Division, Lawrence Berkeley National Laboratory

*To whom the correspondence should be addressed

Abstract: A nano-catalyst comprised of oxidized Co NPs supported on MgO nano-plates was synthesized via a hydrothermal co-precipitation strategy and a calcination in O_2 and sequential H_2 atmospheres at 250ºC. Spectro-microscopic characterization was performed with scanning transmission electron microscopy, electron energy loss spectroscopy and scanning X-ray transmission microscopy. Ambient pressure X-ray photoelectron spectroscopy and in situ x-ray absorption spectroscopy allowed surface measurements under H_2 and H_2+CO atmospheres in the 225-480ºC range. These measurements at the atomic and microscopic levels demonstrated that oxidized Co nanoparticles uniformly decorated the MgO nano-plates. Surfaces are enriched with Co, and with mixtures of $Co(OH)_2$ and CoO under H_2 and H_2+CO atmospheres. In H_2 atmospheres, the outermost surfaces were composed of (lattice) O^{2-}, CO_3^{2-} and OH^-. No inorganic carbonates were observed in the bulk. Chemisorbed CO, likely on the oxidized Co surfaces, was observed at the expense of O^{2-} under 300 mTorr H_2+CO (2:1) at 225ºC. Gas phase CO_2 was detected under 32 Torr H_2+CO (2:1) at 225ºC upon prolonged reaction time, and was attributed to a surface chemical reaction between O^{2-} and chemisorbed CO. Furthermore, sp^3 like carbon species were detected on an otherwise carbon free surface in H_2+CO, which remained on the surface under the subsequent reaction conditions. The formation of sp^3 like hydrocarbons was ascribed to a surface catalytic reaction between chemisorbed CO and OH^- as the apparent hydrogen source.

Introduction

Nanoparticles of transition group metals and their oxides, owing to their mainly large surface-to-volume ratios, are often employed as catalysts in fundamental research as well as industrial and petrochemical technologies. Nanoparticle catalysts with controlled surface properties such as size, shape, morphology, coordination, and atomic arrangement and orientation are key to understanding catalytic processes [1]. It is often one or some combination of these surface properties that give rise to catalysts with distinct chemical and electronic structures, and ultimately leads to unique catalytic behavior [2].

Co is one such catalyst over which hydrogenation of CO and/or CO_2 is carried out [3]. In the last decade, synthetic routes have been developed to produce nanoparticles of Co with controlled properties [4–6]. However, it was soon realized that the presence of surface capping and directing ligands, which are essential to colloidal synthesis routes, had detrimental effects on catalytic turnovers. This was first demonstrated for hydrogenation of CO_2 for which phospine-based ligands (trioctyl phospine oxide) were identified as catalytic inhibitors [6]. To this end, oleic acid capped Co NPs were supported on mesoporous SiO_2, and tested towards hydrogenation of CO_2 where CO and CH_4 were produced [6].

High surface area supports are essential to catalytic performance in this case. Silicon or metal oxides are often used to disperse active nanoparticle catalyst, and may act as co-catalysts through catalytic bi-functionality such as co-adsorption of reactants; and metal-oxide interactions. For example, a reducible oxide support like TiO_2 was found to enhance catalytic performance for hydrogenation of CO and CO_2 compared to an inert support like SiO_2 over oxidized Co NPs [7]. It was shown that oxidized Co can effectively wet TiO_2 surfaces, when combined with other structural factors, yielding improved catalytic properties. Likewise, non-reducible oxide supports with strong adsorption of CO and CO_2 are expected to lead to unprecedented catalytic performance towards hydrogenation of such gases. Nano-sized MgO is a well-known catalyst support and co-catalyst for CO_2 reforming of methane [8,9] and low temperature oxidation of CO [10], and furthermore forms inorganic carbonates from atmospheric CO and CO_2 [11,12].

In situ probing allows for surface characterization of supported nanoparticle under conditions pertinent to catalytic reactions [2]. Nanoparticles and supports are meta-stable catalysts and as such are trapped in some kinetically-stabilized state. Their surface oxidation state, bonding and coordination are subject to alteration under reactive gas pressures and at elevated temperatures [13]. Ambient pressure X-ray photoelectron spectroscopy (APXPS) and in situ X-ray absorption spectroscopy (XAS), which can be operated under catalytically relevant temperature and pressures naturally allows for in situ probing of structural dynamics.

As yet, no catalytic inhibition effect has been associated with fatty acids used for surface passivation of size-controlled and supported Co (oxide) NPs. To the best of our knowledge, no carbon-free in situ probing of immediate Co (oxide) surfaces has ever been achieved. Synthetic routes and strategies like those that are employed by hydrothermal synthesis platform will lead to ligand free synthesis of size-, shape, and morphology-controlled nanoparticles and supports of metal oxides. These are keys to understanding control of surface factors while rendering high catalytic performance.

Our hypothesis is that surface inorganic carbonates, either pre-formed or generated in situ, could assist in reaction of CO and H_2 at the Co (oxide) interface. Thus as a result they may promote catalytic performance of Fischer-Tropsch synthesis catalysts. This hypothesis was tested using in situ surface techniques over uniform and contamination free NPs of Co (oxides) dispersed over a high surface area MgO support. These were synthesized using a hydrothermal synthesis route and an in situ post-treatment under redox gases, first O_2 and then H_2. As-synthesized and post-reaction catalysts were characterized using micro-spectroscopic tools such as scanning transmission electron microscopy (STEM), electron energy loss spectroscopy (EELS) and scanning X-ray transmission microscopy (STXM), while dynamic surface properties were investigated via in situ surface probes such as APXPS and XAS. Hydrothermal synthesis of a size and composition uniform CoO/MgO nano-catalyst provided for catalytic performance demonstrated in transforming CO at 225ºC to CO_2 and some sp^3-like hydrocarbons.

Experimental

Materials: $Co(NO_3)_2.7H_2O$ (Aldrich) and $Mg(NO_3)_2.6H_2O$ (Strem Chemicals), NaOH (Strem Chemicals) were used as received.

Synthesis of Cobalt Magnesium Oxides: Synthesis of cobalt magnesium oxides was modified from the hydrothermal synthesis of magnesium oxide nano-plates reported by Qian and co-workers [14]. To synthesize the CoO/MgO nano-composite, 23.3 mg $Co(NO_3)_2.7H_2O$ and 227.4 mg $Mg(NO_3)_2.6H_2O$, yielding a total of 0.2 mmol metal salt precursors, were dissolved in 20 mL deionized water (MilliQ) along with 1.0 g of NaOH via sonication. 16 mL of the mixed salt solution was transferred to a stainless steel reactor with a Teflon insert along with a Teflon coated stirring bar. The reactor was sealed and placed in a mineral oil bath maintained at 150ºC and allowed to stir for 16 hours followed by reaction quenching on an ice bath. A brownish colloidal suspension was collected upon centrifugation at 4100 rpm and washed with ethanol:acetone (10:90 v/v). The brown powder was dried at 60ºC for 12 hours. The samples were stored in air at 25ºC until further use.

Techniques: In situ XAS was performed using the detection of electrons, photons, ions for chemistry and catalysis (DEPIC^2) roll-up end-station [15] at beamline 6.0.2 in the Advanced Light Source (ALS). A Ambient pressure cell for the DEPIC^2 is described elsewhere [15]. Total electron yield (TEY) was measured by collecting electron flow (0.05-0.5 nA) from ground to sample current collector via a pico-amplifier (SRS). A positive bias (250-300 V) was also applied 1 mm above the current collector to extract electrons. Energy normalization was done using current reading on the exit slit (30 μm). Co L_3, Mg K, O K and C K edges were monitored in vacuum, under gas pressures and in the 25-250ºC range. H_2 and O_2 pressures were about 10 Torr, $CO+H_2$ (1:2) pressure was about 15 Torr. Chemical compositions of Co was determined via a least-square fitting of the data to Co references.

APXPS measurements were carried out at beamline 9.3.2 in the ALS. CASAXPS software was used for data and error analysis. Two photon energies, 350 eV and 630 eV, were used for the measurements. O 1s, C 1s and Mg 2s + Co 3p were monitored in vacuum, under reactive gas pressures in the 150-480ºC range. H_2 and O_2 pressures were 100 mTorr, $CO+H_2$ (1:2) pressure was 300 mTorr. Mg 2s and Co 3p XPS spectra were used to calculate the surface fractions of Co, where areas under the XPS peaks were normalized with the respective photoionization cross-sections of elements at given photon energies, following Yeh and Lindau [16]. Inelastic mean free paths of photoelectrons were calculated from the TPP2M formula of Tanuma, Powell and Penn for CoO and MgO at the two photon energies employed [17]. The samples used in the XAS and APXPS studies were prepared by casting ~500 μL of an ethanol solution (~1 mg/mL) of CoO/MgO powder onto a silicon wafer. APXPS survey spectra obtained at 250ºC in 100 mTorr O_2 and 100 mTorr H_2 and using 630 eV photons are shown in supporting figure S1.

The molecular and environmental sciences (11.0.2) beamline was used for the scanning transmission X-ray microscopy (STXM) measurements. A 25 nm zone plate was employed for the experiments on the pre- and post-reaction CoO (10 % atom)/MgO samples. Samples were prepared

by drop casting the powder samples in ethanol (~1 mg/mL) over a Si_3N_4 window (5 mm x 5 mm membrane with 100 nm thickness, Silson, Inc.). Atomic composition of Co was calculated from background subtracted optical density at white light maxima, 780 eV for Co and 1315 eV for Mg, using the Beer-Lambert Law. X-ray absorption cross-sections and absorption edge jumps at the given photon energies were calculated based on data from McMaster et. al [18].

TEM images and STEM/EELS maps/spectra were acquired using a Jeol2100F microscope equipped with a GATAN Tridem EELS spectrometer at the imaging and manipulation facility in the Molecular Foundry. An accelerating voltage of 200 kV was used for both the TEM and STEM/EELS. EELS resolution was 1 eV, measured as FWHM of zero loss peak in vacuum, and collection angle was 12 mrad.

Results

1. Microscopic and Spectro-microscopic Characterization of the As-synthesized CoO/MgO Nano-composites

Size and morphology of CoO/MgO system were characterized using TEM, and shown in figures 1a-c for the CoO (10 atom %)/MgO particles. It was found that 1-5 μm aggregates of plate-like grains of MgO with ~50 nm diameter and ~10 nm thickness was formed during hydrothermal synthesis. High magnification bright field TEM images (Figure 1b) indicated lamellar nature of the plate-like particles. Annular dark field images (i.e. z-contrast images in Figures 1c and 1f) revealed 5.1 (±1.2) nm particles, identified as Co nanoparticles judged from their brighter contrast.

STEM/EELS spectra in Figure 1e acquired from various locations (Figure 1c) indicated a broad distribution of O/(Mg + Co) and Mg/(Mg + Co) in the 0.2-0.8 range, suggesting local fluctuations in the elemental composition. Co L3/L2 ratios were found to be uniform (2.9±0.2), and revealed predominantly Co^{2+} (Figure 1e). STEM/EELS mapping of a bunch of plate-like particles (Figures 1f) indicated random and uniform distribution of Co, Mg and O elements. This also revealed discrete nanoparticles (NPs) of Co, as shown in figure 1g for the CoO (10 % atom)/MgO system. Fractions of O and Co were calculated from Hartree-Slater formalism via GATAN GIF software. Co L_3/L_2 edge ratios were calculated based on a procedure reported in reference [19].

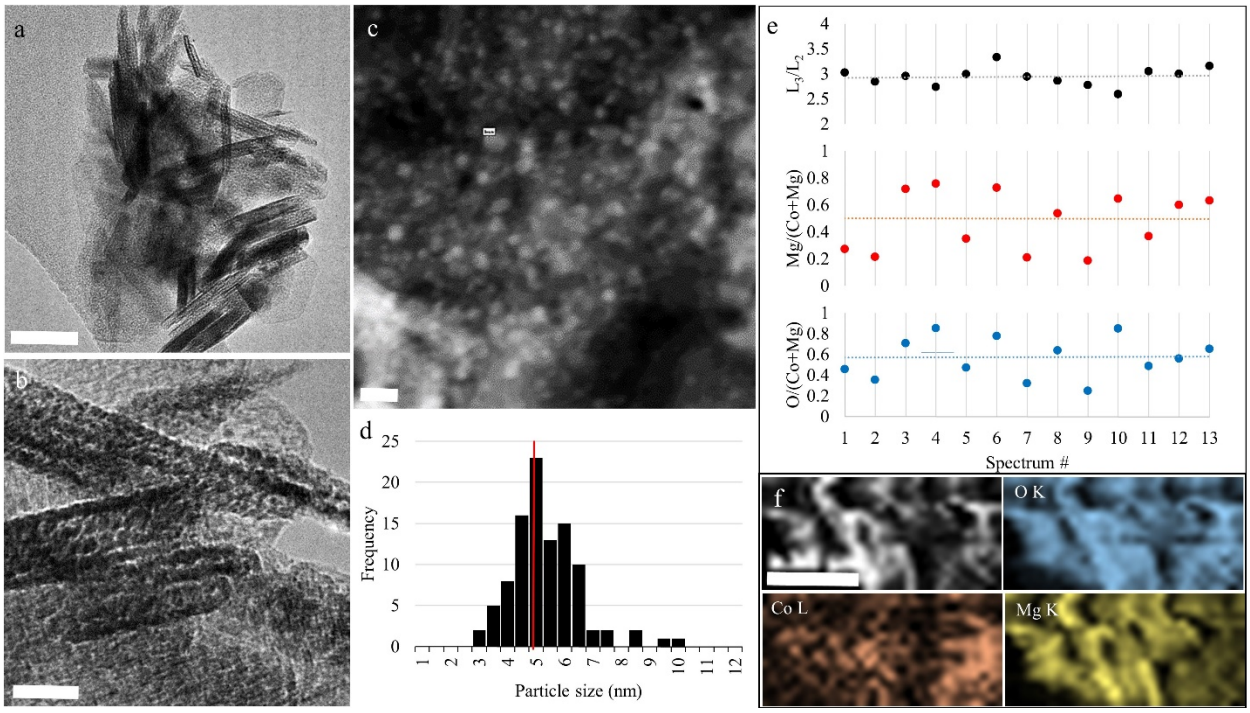

Figure 1. (a) and (b) Bright field TEM images, and (c) annular dark field STEM image of the as-synthesized CoO/MgO nano-composites. (d) Particle size histogram. e) Plots of Co L_3/L_2 EELS ratios, and ratios of reduced O and Mg EELS signals relative to combined (reduced) Co+Mg signals. (f) STEM image and EELS maps acquired at O K, Co L and Mg K edges. Scale bars are 50 nm in (a), 10 nm in (b), 20 nm in (c) and 50 nm in (f).

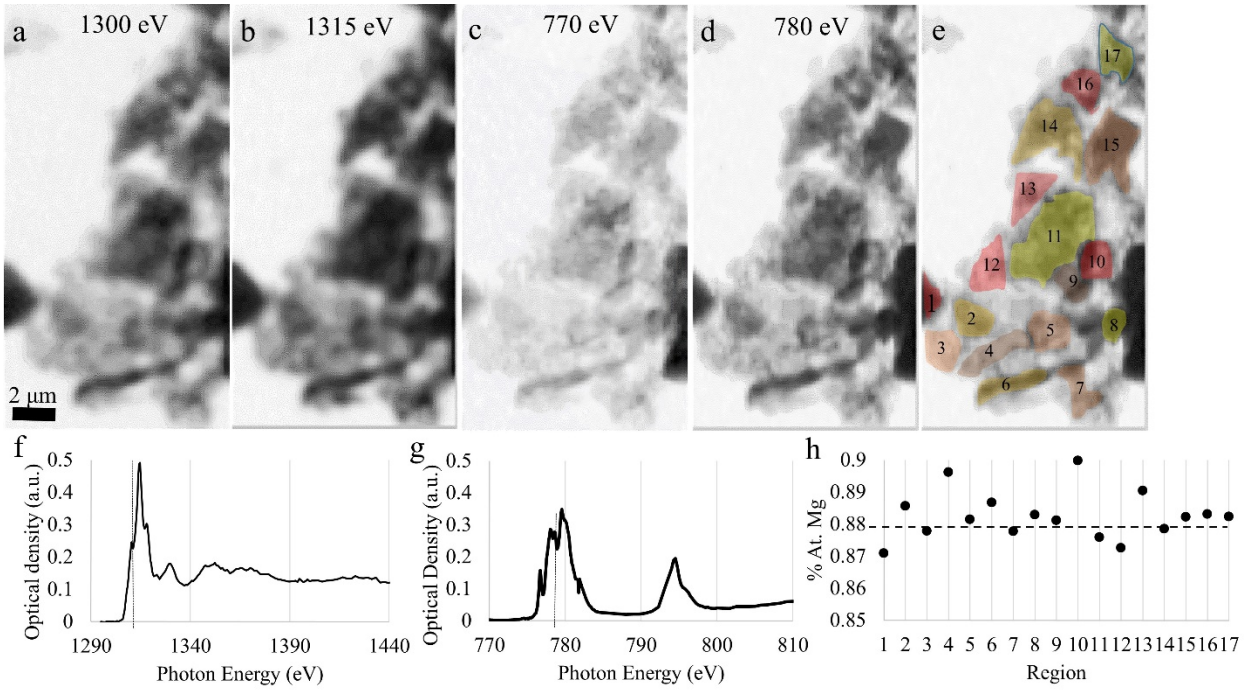

Figure 2. STXM maps acquired (a) Mg K pre-edge, (b) Mg K edge white line maximum, (c) Co L_3 pre-edge, and (d) Co L_3 edge white line maximum. (e) STXM image in (b) superimposed with regions of interest in (h). Representative NEXAFS spectra at (f) Mg K edge and (g) Co $L_{3,2}$ edges taken from region #14. (h) Plots of % at. Mg calculated from regions, numbered and color-coded, in (e).

STXM mapping of a larger aggregate, shown in Figure 2, revealed both compositional and chemical uniformity in the micron scale. For example, the compositions by Mg for the color-coded regions in Figures 2e, were calculated in the range of 87-90 at. % with an average of 88.7 at. % for the whole aggregate (Figure 2h). It was also noted from a qualitative inspection of the color-coded spectra that the as-made Co NPs were composed mainly of $Co(OH)_2$ phase. Similarly, the as-made Mg was identified as phase pure $Mg(OH)_2$ (see Figures 2f and 2g, and the supporting figure S2). $Mg(OH)_2$ was dehydrated, forming MgO phase, following the heat treatment in O_2, whereas $Co(OH)_2$ was maintained in equilibrium with other cobalt oxides, at least on the near-surface regions, under reactive gas atmospheres and at elevated temperatures.

2. In situ X-ray Spectroscopic Investigation

Surface chemical and elemental properties of CoO/MgO system was studied using APXPS and in situ XAS under near ambient H_2 atmospheres in the 250-480ºC range, and in H_2+CO reaction mixtures at 225ºC. XPS spectra in Figure 3a shown in the order of acquisition, Mg 2p [20]and Co 3p shallow core levels under various gas and temperature conditions. The strong peaks at 50 eV were assigned to various Mg species [20,21] . No attempt was made to decompose the Mg 2p spectra into oxide, hydroxide or carbonate components given the symmetric and narrow peak shapes. However, it was noted that peak full width half maxima were systematically broader at 630 eV than 350 eV, and under H_2+CO atmospheres compared to H_2 atmospheres (supporting figures S3). Figure 3b exhibits plots of metal fractions as functions of various conditions at two photon energies (350 eV and 630 eV). It is clear from the spectra and the plots, that near-surface regions are Co richer at 350 eV than 630 eV with corresponding mean photoelectron free paths of 9 and 14 Å. These values are for MgO and about 20% shorter for CoO.

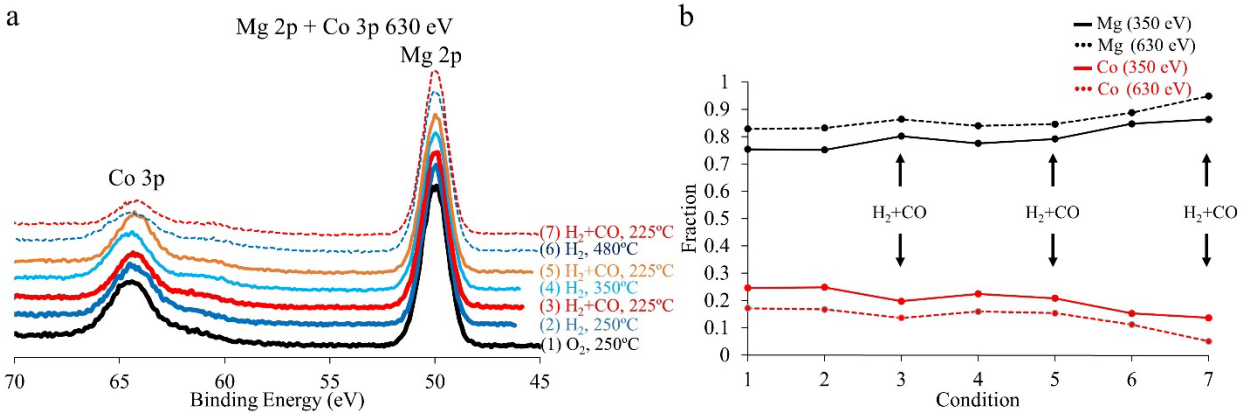

Figure 3. (a) Mg 2p+Co 3p XPS spectra are shown under various conditions. (b) Plots of fractions of Mg and Co at two photon energies. XPS spectra in (a) were acquired progressively from bottom to top.

Surface fraction of Co remained above the bulk value in H_2 at the 250-350ºC range, and during the H_2+CO reaction. However, H_2 treatment at 480ºC caused a substantial decrease in the surface fractions of Co, which was maintained during the subsequent reaction. STEM/EELS maps acquired for the spent CoO/MnO catalyst, shown *vide supra* in Figure 6, indicated sintering of Co NPs, which increased particle size to about 15 nm. This size growth accounts for the drop in surface fractions of Co measured by APXPS.

In situ XAS, probing the near surface regions several nanometers deep, showed that for Co (Figures 4a and 4b) an equimolar mixture of Co_3O_4 and $Co(OH)_2$ in H_2 at 250ºC. This was also shown during the subsequent reaction for Co while CoO was formed at the expense of Co_3O_4 in H_2 at 350ºC. CoO was also detected after 11 hours under H_2+CO mixture following the H_2 treatment at 250ºC. O K-edge XAS, shown in Figure 4d, indicated a decrease in lattice oxygen (O^{2-}) while C K-edge XAS, shown on Figure 4c, indicated CO_2 in the gas phase, which overlapped with the formation of CoO from Co_3O_4.

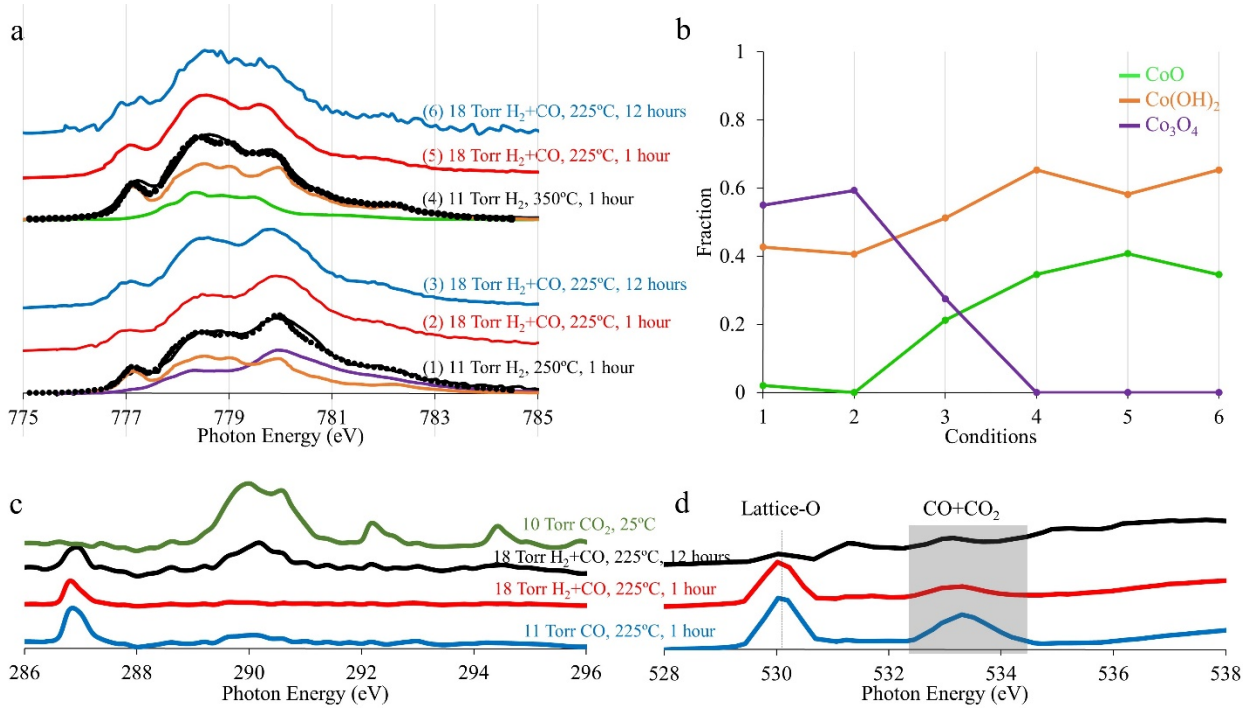

Figure 4. (a) In situ XAS spectra at Co L_3 absorption edge acquired under various conditions. (b) Plots of fractions of various Co species caclulated from XAS spectra in (a). In situ XAS spectra at (c) C K and (d) O K absorption edges acquiered under given conditions. Linear combination fits and components for two conditions are given in (a). Co species were color-coded in (a) and (b). Positions of lattice oxygen and gas phase $CO+CO_2$ were marked in (d).

APXPS was employed to study surface ad-layers under reaction conditions. Figure 5a shows C 1s XPS spectra under reactive gas atmospheres and at elevated temperatures. It was found in O_2 and subsequently in H_2 at 250ºC that the outermost surfaces are composed of CO_3^{2-} (290.2 eV). O 1s XPS spectra, shown in Figure 5c, indicated CO_3^{2-} (533.8 eV) and OH^{-1} (532.0 eV) along with O^{2-} (530.5 eV) under identical conditions, in qualitative agreement with the literature [22]. The high binding energy peak at 534.3 eV was observed only during the initial O_2 oxidation and H_2 reduction treatments at 250ºC, and assigned to surface NO_2^- species [23]. In support of this assignment, APXPS survey spectra acquired under identical conditions showed NO_2^- at 408 eV (supporting figure S1). No $MgCO_3$ phase was apparent from in situ XAS. However, CO_3^{2-} was ascribed locally to MgO surfaces, and no bulk $Mg(OH)_2$ was present at this point. During the H_2+CO reaction at 225ºC, additional peaks for adsorbed CO and gas phase CO appeared in both C 1s and O 1s spectra. The former peak was tentatively attributed to CoO surfaces. It was also noted that, in C 1s XPS spectra, sp^3-like carbon species (285.5 eV) were detected after H_2+CO was first introduced at 225ºC; prior to that C 1s spectra were clean of carbon besides CO_3^{2-}.

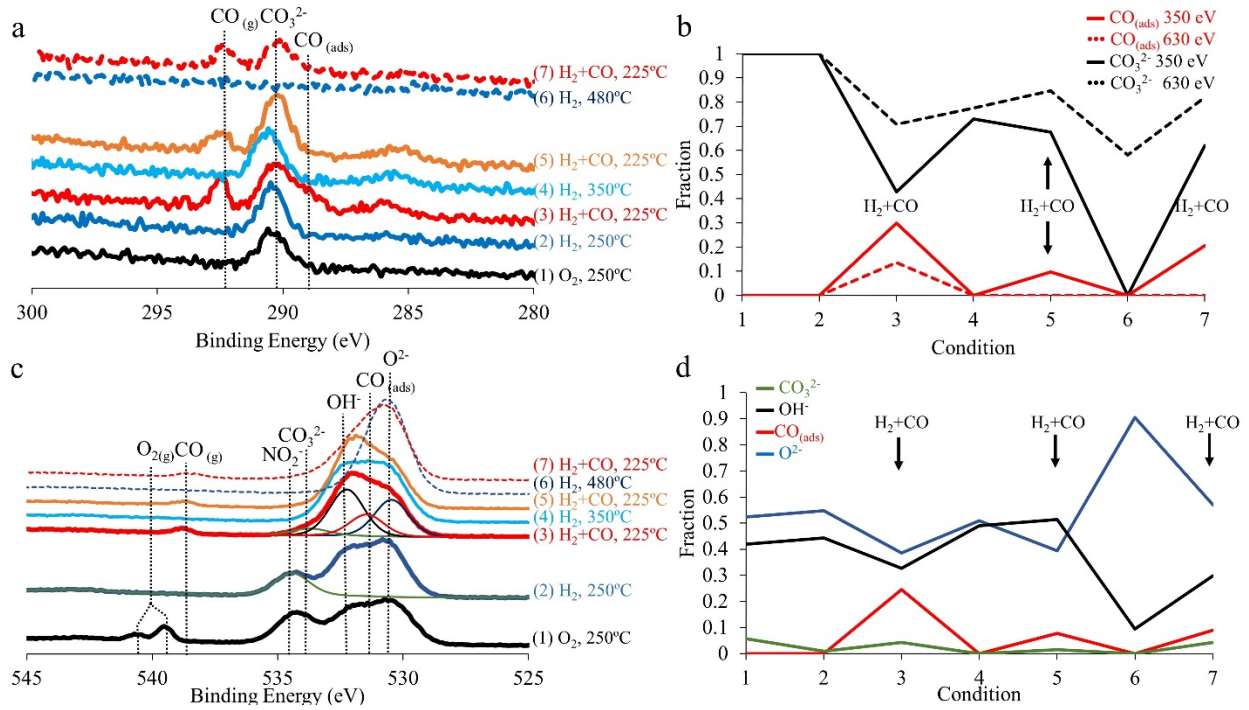

Figure 5. (a) C 1s APXPS spectra acquired using 350 eV photons and under various conditions. (b) Plots for fractions of adsorbed CO ($CO_{(ads)}$) and lattice carbonate (CO_3^{2-}) using two photon energies. (c) O 1s APXPS spectra under various conditions. (d) Plots for fractions of various O species. Binding energies of adsorbed CO, lattice carbonate and gas phase CO are marked in (a). Binding energies of lattice oxygen, adsorbed CO, lattice carbonate, lattice hydroxide, adsorbed water, and gas phase CO and O_2 are marked in (c).

It was found that adsorbed CO formed at the expense of O^{2-} (Figure 5d), in qualitative agreement with in situ XAS. Surface fraction of CO_3^{2-} dropped in favor of adsorbed CO during the H_2+CO reaction. However, actual C 1s (and O 1s) counts for CO_3^{2-} did not change until H_2 treatment at 480ºC; O 1s peak for OH^- disappeared in H_2 and at 480ºC, only to reappear under the subsequent H_2+CO reaction. It was also found that CO_3^{2-} irreversibly shifted to lower binding energies (533.8 eV), in quantitative agreement with the reference [22], during the H_2+CO reaction at 225ºC following the H_2 treatment at 250ºC. Also of note, adsorbed CO (288.8 eV) was more prominent at 350 eV than 630 eV Figure 5b and supporting figure S4, indicating that it was truly an ad-layer localized to outermost surfaces.

3. Microscopic and Spectro-microscopic Characterization of the post-reaction CoO/MgO Nano-composites

A representative STEM/EELS map is shown in Figure 6b. It was apparent from the Co L EELS map that Co signal was localized and indicated larger NPs than the as-synthesized CoO/MgO nano-composites. Figures 6b shows the surface plots of the respective elements; and Figure 6c are the EELS spectra taken at two points and marked with color-code on Figure 6a. STEM/EELS clearly demonstrated that the post-reaction CoO/MgO exhibited segregation and sintering of Co NPs.

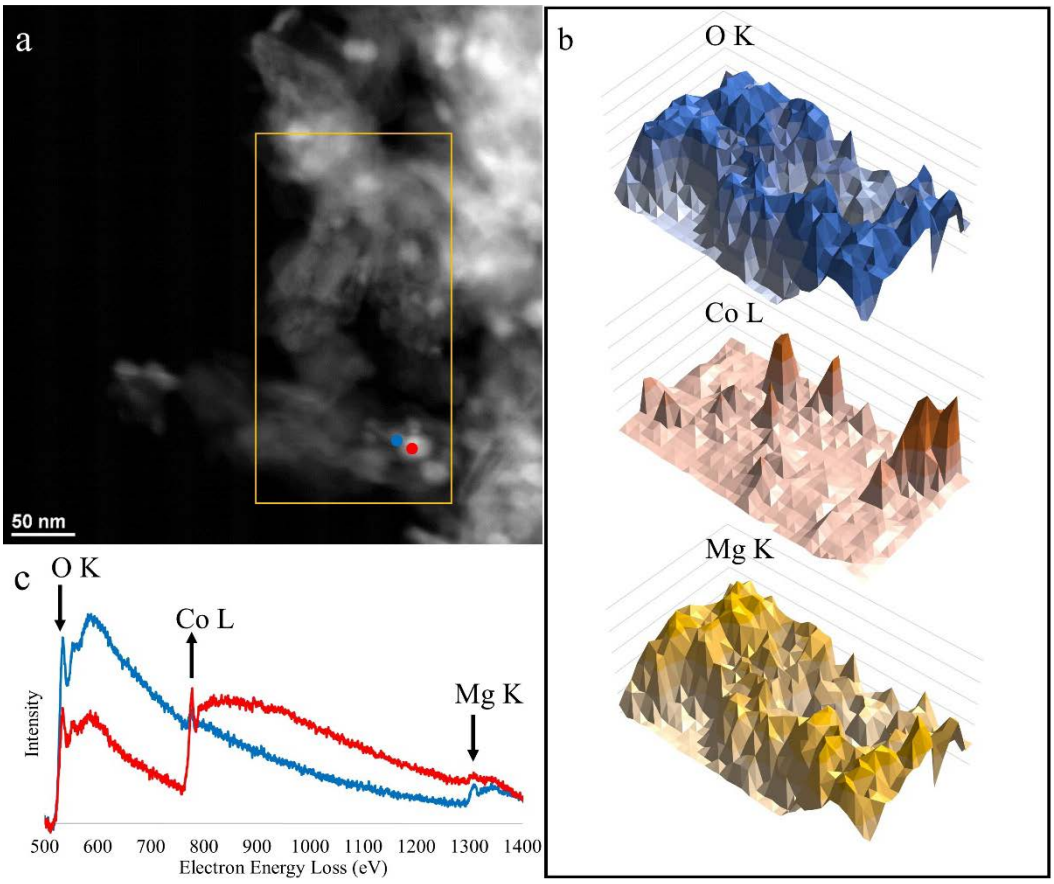

Figure 6. (a) STEM image of the post-reaction CoO/MgO nano-composites. (b) 3D surface curves of EELS maps at O K, Co $L_{3,2}$ and Mg K edges (from top to bottom) acquired from the enclosed region in (a). (c) EELS spectra obtained from two points marked and color-coded in (a).

STXM maps, acquired at both Co L-edge and Mg K-edge, were used to determine the phase and valence of the respective elements. Figures 7a and 7b shows the STXM map at 1315 eV of a large aggregate, which is similar in size, morphology, and composition to the one depicted in Figure 2. Near edge and extended edge X-ray absorption fine structures, Figure 7e and 7f, respectively, are also shown for the as-synthesized and post-reaction CoO/MgO nano-composites. NEXAFS indicated that the as-synthesized $Mg(OH)_2$ phase was converted to MgO after progressive treatments under reactive gases and at elevated temperatures (Figure 7e). This was demonstrated by changes in magnitude and phase of EXAFS oscillations (Figure 7f). Moreover, $Co(OH)_2$ was the sole phase post-reaction, indicated by Co L-edge NEXAFS in Figure 7d.

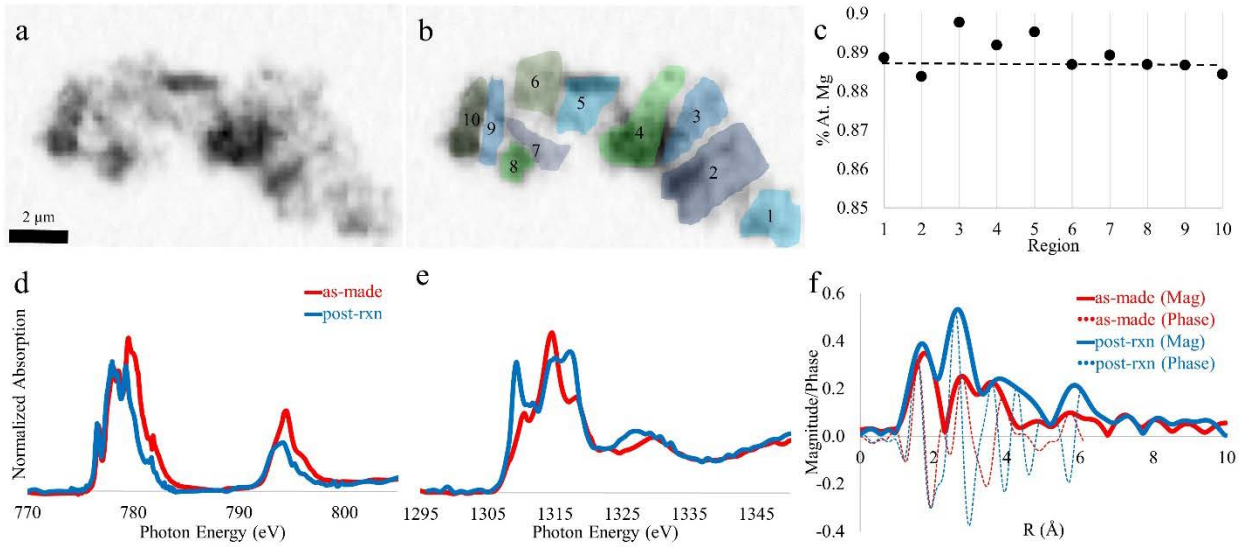

Figure 7. (a) Post-reaction STXM image at Mg K edge white line maximum. (b) the same STXM image in (a) superimposed with regions of interest in (c). (c) Plots of % at. Mg calculated from regions marked and color-coded in (a). Normalized NEXAFS spectra at (d) Co $L_{3,2}$ and (e) Mg K edges comparing, and (f) magnitude and phase of EXAFS oscillations at Mg K edge comparing the as-synthesized and post-reaction samples. Normalized NEXAFS spectra were integrated from the entire grains shown in (a) and Figure 2.

Discussion

CoO nanoparticles catalysts supported on MgO nano-plates were prepared via both one pot synthesis and hydrothermal strategy. The as-made particles were identified as mixtures of Co_3O_4 and $Co(OH)_2$ decorating $Mg(OH)_2$ that transformed to mixtures of CoO and $Co(OH)_2$ with a representative formula unit of $CoO_x(OH)_{2-2x}$, and MgO after O_2 and subsequent H_2 treatments both carried out at 250ºC. Nitrite species were also found on the surface under these conditions, which subsequently decomposed and disappeared as the reaction evolved. The elemental composition of the as-made nano-composite particles were 11 at. % by Co and uniform across micron-sized grains of MgO nano-plates, but exhibited local variations in the nano-size, giving rise to up to 50 at. by Co. This was measured through Co NPs.

Co was found to cover surfaces of MgO nano-plates, and hence led to 20 at. % of near surface regions. Surface concentration and particle sizes of Co remained almost unchanged in H_2 up to 350ºC and during the H_2+CO reaction at 225ºC. This makes the CoO/MgO nano-composite catalyst potentially very attractive towards hydrogenative reforming reactions. However, an abrupt drop on surface coverage of Co was observed upon H_2 treatment at 480ºC and the subsequent reaction under H_2+CO. This indicated that, in H_2 and above 350ºC, support interaction was weak and lost to sintering of Co.

The outermost surfaces of CoO/MgO nano-composites were investigated using APXPS in H_2 and H_2+CO conditions to evaluate their potential as catalysts towards hydrogenative reforming of CO, i.e. Fischer-Tropsch synthesis. The results are summarized in Schematic 1. First, under all

conditions studied, CO_3^{2-} was found on the near surface regions. It was anticipated that the starting $Co(OH)_2/Mg(OH)_2$ nano-composites, through high surface Mg oxides/hydroxides, absorbed CO_2 gas and formed CO_3^{2-} on the near surface regions. XAS (TEY) and STXM did not show any CO_3^{2-} phase as these techniques were not as sensitive to the outermost surfaces compared to APXPS. CO_3^{2-} was completely purged from the outermost surfaces, but retained in diminished concentration on the near surface regions up to 480ºC in H_2. The availability and accessibility of CO_3^{2-} at the interface with Co oxides/hydroxides is an intriguing option for production of oxygenates from syngas, however, it appears that the stability of lattice carbonates renders the use of MgO support difficult in such a catalytic reaction scheme.

Schematic 1. A summary of the surface evolution of nano-structured CoO/MgO composite. Symbols up, down and bar represent increase, decrease and no change in fractions, respectively.

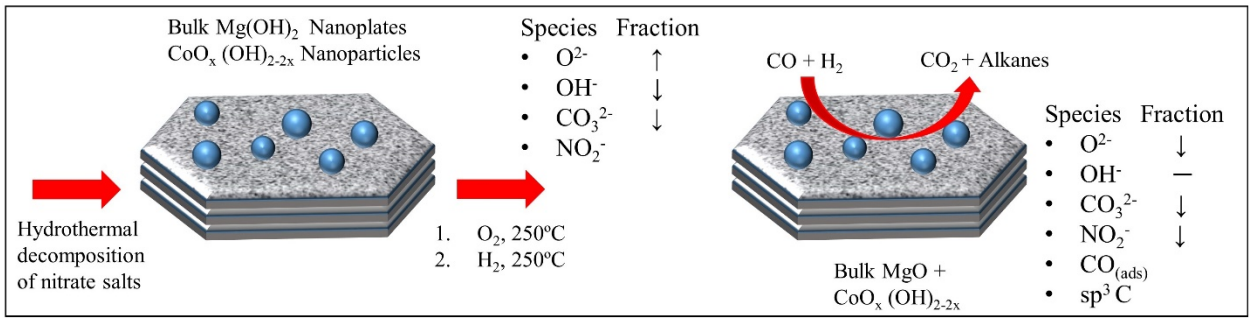

CO adsorbed on the nano-composites on the Co NPs. The adsorption of CO induced a sudden drop in O^{2-}. CO_2 was detected in the gas phase accompanied with a significant drop in lattice oxygen using XAS and TEY under similar conditions. Overlapping results suggested a surface chemical reaction of CO with lattice oxygen. However, the source of lattice oxygen could not be determined conclusively. The evidence suggested that both CoO and MgO could be involved. For example, the fraction of CoO in the near surface regions decreased under H_2+CO mixture in the long reaction time limit compared to identical conditions in the short reaction time (or H_2 environments); and near surface regions were mainly composed of Mg oxides and carbonates.

In addition to CO_3^{2-}, adsorbed OH^- was detected on the outermost surfaces in both O_2 and H_2 atmospheres at 250ºC. Surface fraction of OH^- significantly dropped in H_2 at 480ºC. During the subsequent H_2+CO reaction, OH^- was restored, indicating a surface chemical reaction between lattice O and hydrogen, either in the chemisorbed state or gas phase.

Finally, sp^3-like carbon species formed on the immediate surfaces during the H_2+CO reaction at 225ºC. Also of note is that the outermost surfaces were free of carbon prior to the dose of H_2+CO. This could be an indication of a catalytic reaction of surface adsorbed CO and H. Since no metallic Co was present, the most likely source of H was OH^-, which was present in the form of $Co(OH)_2$.

It has been argued in the literature that formation and stability of carbonate species could be the key to production of oxygenated hydrocarbons during hydrogenation of CO or CO_2. Lattice carbonates are generated on Mg oxides, but can only be detected using surface sensitive techniques. CO could be adsorbed on non-metallic Co surfaces and there is some evidence that

CO reacted with surface hydroxides to produce surface carbon species. CO_2 was also produced over CoO/MgO nano-composites by either a reaction of adsorbed CO with lattice oxygen or decomposition of lattice carbonates under H_2+CO atmospheres at 225ºC. The bonding configuration and orientation of these CO_3^{2-} species are not clear from our current study, and warrants vibrational spectroscopic investigations.

Conclusion

A nano-composite of CoO NPs supported over MgO nano-plates was prepared via a hydrothermal synthesis and a subsequent solid-state calcination at 250ºC in first O_2 and then H_2. The as-synthesized nano-composites were characterized by electron and X-ray spectro-microscopic tools in the nano and sub-micron scales. 2-5 nm particles composed mainly of $Co(OH)_2$ were found to be uniformly distributed over 50-100 nm wide, 5-10 nm thick $Mg(OH)_2$ nano-plates. STXM of large aggregates indicated a uniform distribution with an average of 88 % at. Mg whereas STEM/EELS indicated local variations in distribution of O and Co elements.

Binary nanocomposites were investigated in O_2, H_2 and H_2+CO atmospheres based on in situ spectroscopy using synchrotron X-rays. It was found that nanoparticles with a representative formula unit of $CoO_x(OH)_{2-2x}$ were decorating MgO surfaces, and remained uniform up to 480ºC in H_2. The post-reaction spectro-microscopic investigation revealed an increase in particle sizes of CoO NPs due to sintering, while maintaining long range distribution. This is in agreement with loss in surface fraction of Co.

The outermost surface layers were probed by APXPS, and determined to be covered with hydroxides and inorganic carbonates. CO was found to be sticking to surfaces comprised of hydroxides and oxides under the H_2+CO conditions. Also during the H_2+CO reaction, lattice oxygen was consumed in favor of adsorbed CO and hydroxides. Along with a drop in lattice oxygen, gas phase CO_2 was detected after a prolonged reaction. Overlapping results pointed to a surface chemical reaction scheme: (i) adsorbed CO reacted with lattice oxygen and desorbed as CO_2; (ii) lattice carbonates decomposed to gas phase CO_2 and lattice oxygen, which, in return, reacted with adsorbed CO to further produce CO_2; or (iii) some combination thereof. Furthermore, sp^3-like carbon species on immediate surfaces were observed under the H_2+CO conditions, attesting to a catalytic reaction pathway between adsorbed CO and hydroxides as the apparent hydrogen source.

References

1 G. A. Somorjai and J. Y. Park, *Angew. Chem.-Int. Ed.*, 2008, **47**, 9212–9228.
2 S. Alayoglu, J. M. Krier, W. D. Michalak, Z. Zhu, E. Gross and G. A. Somorjai, *Acs Catal.*, 2012, **2**, 2250–2258.
3 G. L. Bezemer, J. H. Bitter, H. Kuipers, H. Oosterbeek, J. E. Holewijn, X. D. Xu, F. Kapteijn, A. J. van Dillen and K. P. de Jong, *J. Am. Chem. Soc.*, 2006, **128**, 3956–3964.
4 S. H. Sun and C. B. Murray, *J. Appl. Phys.*, 1999, **85**, 4325–4330.
5 V. F. Puntes, K. M. Krishnan and A. P. Alivisatos, *Science*, 2001, **291**, 2115–2117.
6 V. Iablokov, S. K. Beaumont, S. Alayoglu, V. V. Pushkarev, C. Specht, J. Gao, A. P. Alivisatos, N. Kruse and G. A. Somorjai, *Nano Lett.*, 2012, **12**, 3091–3096.

7 G. Melaet, W. T. Ralston, C.-S. Li, S. Alayoglu, K. An, N. Musselwhite, B. Kalkan and G. A. Somorjai, *J. Am. Chem. Soc.*, 2014, **136**, 2260–2263.
8 D. Qin and J. Lapszewicz, *Catal. Today*, 1994, **21**, 551–560.
9 B. Q. Xu, J. M. Wei, H. Y. Wang, K. Q. Sun and Q. M. Zhu, *Catal. Today*, 2001, **68**, 217–225.
10 J. L. Margitfalvi, A. Fasi, M. Hegedus, F. Lonyi, S. Gobolos and N. Bogdanchikova, *Catal. Today*, 2002, **72**, 157–169.
11 S.-W. Bian, J. Baltrusaitis, P. Galhotra and V. H. Grassian, *J. Mater. Chem.*, 2010, **20**, 8705–8710.
12 F. Khairallah and A. Glisenti, *J. Mol. Catal. -Chem.*, 2007, **274**, 137–147.
13 F. Tao, M. E. Grass, Y. Zhang, D. R. Butcher, J. R. Renzas, Z. Liu, J. Y. Chung, B. S. Mun, M. Salmeron and G. A. Somorjai, *Science*, 2008, **322**, 932–934.
14 Y. Ding, G. T. Zhang, H. Wu, B. Hai, L. B. Wang and Y. T. Qian, *Chem. Mater.*, 2001, **13**, 435–440.
15 W. T. Ralston, N. Musselwhite, G. Kennedy, K. An, Y. Horowitz, A. A. Cordones, B. Rude, M. Ahmed, G. Melaet and S. Alayoglu, *Surf. Sci.*
16 J. Yeh and I. Lindau, *At. Data Nucl. Data Tables*, 1985, **32**, 1–155.
17 Tanuma S., C. J. Powell and D. R. Penn, *Surf. Interface Anal.*, 2011, **43**, 689–713.
18 W. H. McMaster, N. K. Del Grande, J. H. Mallett and J. H. Hubbell, *Compilation of X-Ray Cross Sections.*, California Univ., Livermore. Lawrence Radiation Lab., 1969.
19 C.-S. Li, G. Melaet, W. T. Ralston, K. An, C. Brooks, Y. Ye, Y.-S. Liu, J. Zhu, J. Guo, S. Alayoglu and G. A. Somorjai, *Nat. Commun.*, 2015, **6**, 6538.
20 F. Khairallah and A. Glisenti, *Surf. Sci. Spectra*, 2006, **13**, 58–71.
21 V. Fournier, P. Marcus and I. Olefjord, *Surf. Interface Anal.*, 2002, **34**, 494–497.
22 D. K. Aswal, K. P. Muthe, S. Tawde, S. Chodhury, N. Bagkar, A. Singh, S. K. Gupta and J. V. Yakhmi, *J. Cryst. Growth*, 2002, **236**, 661–666.
23 E. Ozensoy, C. H. F. Peden and J. Szanyi, *J. Phys. Chem. B*, 2005, **109**, 15977–15984.

Acknowledgements

This work is supported by the Director, Office of Science, Office of Basic Energy Sciences, of the US Department of Energy under contract DE-AC02-05CH11231. TEM and STEM/EELS measurements were performed at the imaging and manipulation facility in the Molecular Foundry. STXM, APXPS and XAS experiments were carried out in the Advanced Light Source. SA thanks Mr. Walter Ralston, Dr. Gerome Melaet and Dr. Ethan Crumlin for their help during the APXPS data acquisition.

Graphical abstract